IEEE Control Systems Letters paper presented at
2023 American Control Conference (ACC)
San Diego, CA, USA. May 31 - June 2, 2023

Adaptive Online Fault Mitigation using Hierarchical Engine Control

Dhrubajit Chowdhury, Raman Goyal, Raj Pradip Khawale, Lara Crawford and Rahul Rai

***Abstract*— This paper proposes a hierarchical control architecture to mitigate faults and modeling errors in an engine system. A hybrid approach is used to model the complete engine system with the main cylinder combustion process represented using a neural network model and the rest of the system is modeled using well-studied physics-based analytical equations. A control calibration map that consists of the optimal engine control parameters to maintain the desired engine torque using the minimum fuel consumption rate is generated offline by performing Bayesian optimization on this high-fidelity hybrid engine model. We then use proportional-integral (PI) and extremum seeking (ES) controllers on top of the offline map to compensate for any engine faults and modeling errors for online calibration. The work is motivated by optimally reconfiguring autonomous systems. We test three different scenarios through numerical simulations which require online calibration of the engine control parameters. It is shown that the PI+ES controller can overcome the fault by maintaining the desired torque and also lowers the fuel consumption rate compared to a PI controller.**

I. Introduction

Autonomous systems cannot be completely autonomous until they can handle faults in their operation. The U.S. Navy has an increasing interest in using unmanned surface vessels for long-duration voyages and is interested in autonomous vessels that can adapt to and mitigate faults, so they will not need rescue even when something goes wrong. This will mandate more sophisticated fault diagnosis and fault mitigation algorithms to manage the ship's machinery and electrical systems when there is no one on board to address them. This reasoning applies to all autonomous systems, particularly those that have high-level goals specified and are required to make decisions on their own to best attain these goals. Even if faults are identified, autonomous systems do not typically have the models or reasoning to adapt appropriately to the new situation.

The main motivation for this research work comes from the need to autonomously mitigate the engine faults to successfully complete the mission [1]. Although many maritime vessels use diesel engines due to their reliability and efficiency, it is still of utmost importance to reason over the engine's own health and take remedial action if faults are present [2]. The paper will mainly focus on generating online control calibration maps and mitigating faults such as cavitation and the clogging issue of fuel injectors, the existence of disturbance at the onset of injection, etc., and will provide a hierarchical engine control framework to mitigate these faults in an online fashion. The fault mitigation strategy will involve finding the optimal set of fuel injection parameters to overcome the effects of these faults and still achieve the higher level objective of the vessels, i.e., to achieve the desired ship speed necessary for the mission. This paper will develop the online fault mitigation framework with the primary objective being to command the desired torque from the engine while increasing the fuel efficiency, i.e., to minimize the fuel consumption rate to best enable mission completion in the presence of a fault.

D. Chowdhury, R. Goyal, and L. Crawford are with Palo Alto Research Center - A Xerox Company, Palo Alto, CA, USA. R. Khawale and R. Rai are with the Department of Automotive Engineering, Clemson University, Clemson, SC, USA. {chowdhury, rgoyal, lcrawford}@parc.com, {rkhawal, rrai}@clemson.edu

A. Literature Review

In diesel engines, fuel efficiency is optimized by controlling the fuel quantity and timing in the combustion phase. The fuel injection system uses electronic control to change the fuel quantity and timing based on a calibrated lookup table. The lookup table stores the values of engine control parameters, namely, injection pressure, injection duration, and the start of injection, which are optimized to achieve maximum fuel efficiency for different engine operating conditions. This control structure is open-loop in nature as the engine control parameters are optimized offline. This structure suffers in practice due to differences in engine modeling errors, non-calibrated operating points and faults appearing during actual operation, which necessitates the need for online feedback control [3].

Extremum seeking (ES) controllers have been used for online calibration of the engine control parameters due to their model-free nature [4]. ES controllers have been used for the optimization of the starting speed in a gasoline engine [5], regulation of intake air for timing optimization in homogeneous charge compression ignition (HCCI) engine [6], optimization of gasoline engine spark timing and air-fuel ratio to minimize a cost function related to the indicated torque, exhaust temperature, and knock intensity [7], and online calibration of a flex-fuel engine system [8]. Other implementations of ES controller for engine optimization include [9], [10], and [11]. A comprehensive review of the optimization algorithms used for engine calibration can be found in [12].

B. Main Contribution

In most of the ES applications, including those referenced in this paper, the cost function considered is the Brake Specific Fuel Consumption (BSFC), which is equal to the fuel flow rate divided by the power produced by the engine. In engine applications, it is very challenging to measure BSFC in practice as the fuel flow rate is not available and

979-8-3503-2806-6/$31.00 ©2023 AACC

needs to be estimated in order to use ES controller [13]. This paper uses proportional-integral (PI) controllers to change the injection pressure and duration to maintain the engine torque at the desired setpoint. The PI controllers use the difference between the setpoint torque and current engine torque as the feedback variable. An ES controller is designed which uses the start of injection (SOI) as the control variable to maximize the engine torque. As the engine torque increases when the ES controller changes the SOI, the PI controllers lower the injection pressure and duration to maintain the torque at the desired setpoint, thereby lowering the fuel consumption rate. Therefore, the ES controller indirectly minimizes the fuel consumption rate by maximizing the engine torque. We test the online calibration optimization and fault mitigation of the PI+ES controller for three different scenarios.

II. Hybrid Engine Model

A. Engine Specifications

The paper develops a high-fidelity hybrid engine model for a 7.6-liter Navistar/International engine installed at Clemson University. The specifications of the engine are given in Table I. This model is tuned and validated over a wide range of experimental data. We calibrate this model for engine speed and torque ranges between 800-2000 RPM and 100-600 Nm, respectively.

TABLE I: ENGINE SPECIFICATIONS

List	Values
Engine Type	Diesel, 4-Cycle
Configuration	In-line 6-cylinder
Displacement	7.6 L
Stroke	119 mm
Bore	116.6 mm
Compression Ratio	16.9:1
Fuel System	High-Pressure Common Rail System

Multiple mean value models with various complexities and states are published for diesel engines [14]–[17]. Particularly, the model from Wahlström and Eriksson [18] is considered as a baseline model, and we improve the fidelity of the model by replacing and adding various components. The structural diagram of the hybrid model is shown in Fig. 1. This model has twelve parameters (depicted in Fig. 1) which capture pressure, mass flow, and temperature within various components of the system along with the total torque generated from the engine.

The control input parameters of the model are as follows:

1) Engine speed (rpm) - n_e
2) Injection pressure (MPa) - u_{Pinj}
3) Injection duration (ms) - u_{tinj}
4) Start of injection (crank angle degree - CAD) - u_{SOI}

The engine model is detailed in the following two subsections.

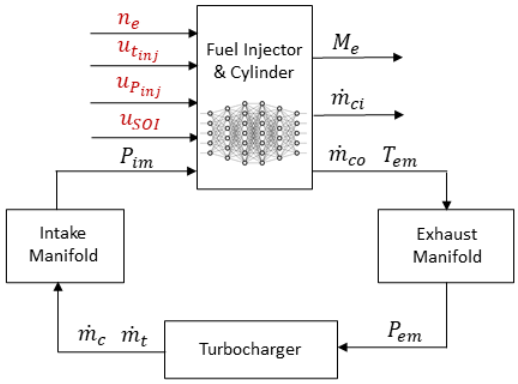

Fig. 1: Hybrid engine model structural diagram

B. Fuel injector and cylinder subsystems

The Navistar engine has a high-pressure common-rail fuel injection system, and the corresponding model captures the fuel mass coming out from the injector using the principle of conservation of mass. The injection flow rate is related to the nozzle flow area, discharge coefficient, and pressure difference. The equation used for modeling the injection flow rate is as follows:

$$Q_{inj} = \alpha.sign(u_{Pinj} - P_{cyl}).c_d.A_{flow}\sqrt{\frac{2}{\rho}|u_{Pinj} - P_{cyl}|}, \quad (1)$$

where α is a binary value used to incorporate injection duration, for instance, the value of α will be one for the mass flow rate between the start of injection (SOI) and end of injection (EOI) and for all other cases, α will be zero. The remaining parameters from eq. 1 are defined in the appendix.

The combustion process is one of the crucial portions of the engine, and improving the fidelity of the combustion model is important for improving the accuracy of the overall diesel engine model. Thus, we started with a detailed thermodynamic cylinder model that simulates the in-cylinder processes and their thermodynamic states for all crank angles during the engine cycle. The model captures various parameters for a complete cycle like intake and exhaust mass flows, torque, in-cylinder pressure, exhaust temperature, oxygen mass fraction, efficiency, power, mean effective pressures, etc. However, this detailed crank angle-based cylinder model is computationally expensive. A faster model is needed to cater to the requirements of the hierarchical controller. Thus, to improve the computational speed of the overall physics-based model, the detailed thermodynamic cylinder model is replaced with a shallow neural network.

A trained shallow neural network reduces the computational simulation time by an order of magnitude. As the high-fidelity thermodynamic cylinder model involved complex mathematical calculations for each crank-angle, replacing it with the surrogate cylinder model helps in improving the computational time significantly. This network is trained over a dataset generated from the thermodynamic cylinder model. The dataset was generated over an entire feasible range of input cylinder parameters.

The surrogate cylinder model exhibited an average mean squared error (MSE) of 3.42×10^{-4} on the test dataset. Additionally, the outputs of the cylinder model give us a difference of less than 5% with experimental data. Altogether, the trained network exhibited good accuracy with a significant improvement in the computational time.

C. Manifolds and turbocharger subsystems

The modeling of the intake and exhaust manifolds is performed with two states: intake and exhaust manifold pressures. We are modeling the pressure using the principle of mass conservation and the ideal-gas law. The differential equations for the intake and exhaust manifold pressures can be described as follows:

$$\frac{d}{dt}p_{im} = \frac{R_a T_{im}}{V_{im}}(\dot{m}_c - \dot{m}_{ci}), \tag{2}$$

$$\frac{d}{dt}p_{em} = \frac{R_e T_{em}}{V_{em}}(\dot{m}_{co} - \dot{m}_t), \tag{3}$$

where all the parameters in eq 2 and 3 are given in the appendix. The turbocharger model is composed of a turbine model, a compressor model, and a turbo inertia model. The turbocharger model is taken from Wahlström and Eriksson [18] and calibrated using the Navistar engine configuration and collected experimental data. A neural network is used only for the cylinder subsystem, while all other subsystems, such as manifolds, turbocharger, and fuel injector, utilize physics-based models.

III. Control Methodology and Engine Faults Background

In this paper, we use two model-free controllers for engine optimization. The Bayesian optimization (BO) algorithm is used offline in order to obtain the optimal engine control parameters using the high-fidelity engine model described in the previous section. The extremum seeking (ES) controller is used in an online setting on top of the nominal optimal engine control parameters found using BO to compensate for modeling errors and engine faults and to minimize fuel consumption. In this section, we provide a brief description of these two algorithms along with the engine faults.

A. Bayesian Optimization

Bayesian optimization (BO) is generally used to find the global maximizer (minimizer) of an unknown objective function $f(\mathbf{x})$ [19]. The function $f(\mathbf{x})$ might not have a closed-form, but it can be evaluated at a query point $\mathbf{x}$. The problem is defined as:

$$\mathbf{x}^* = \arg\max_{\mathbf{x}\in\mathcal{X}} f(\mathbf{x}), \tag{4}$$

where $\mathcal{X}$ is the design space of interest. The BO framework consists of a surrogate model generally constructed using Gaussian process regression. The surrogate model is initialized with a prior belief about the behavior of the unknown objective function. The model is then sequentially refined with new data when the function is evaluated at new query points. The model is refined with Bayesian posterior updating.

Acquisitions functions are used in the BO framework to leverage uncertainty in the posterior which is used to choose the next query point. The acquisition functions provide a trade-off between exploration and exploitation. For exploration, the optima of the acquisition functions are located where the uncertainty is high, and for exploitation, the optima are located where the model prediction accuracy is high. The acquisition functions themselves are multi-modal, but these functions are cheap to evaluate and have closed-form expressions which make them easier to optimize. In a BO algorithm iteration, the next query point to evaluate the function $f(\mathbf{x})$ is obtained by maximizing an acquisition function.

B. Extremum Seeking Controller

The extremum seeking (ES) controller is a model-free approach for adaptive control, which is used for systems where the input-to-output map $f(\mathbf{x})$ is unknown but is known to have an extremum. For a particular input $\mathbf{x} = \mathbf{x}_1$, the output $f(\mathbf{x}_1)$ can be measured. The ES controller is used to find the input that achieves the extremum. ES controller can be used to find the extremum for a dynamic input-to-output map, where the function $f(\mathbf{x})$ is the output of a dynamical system. The first stability analysis using averaging and singular perturbations for an ES controller applied to a general nonlinear dynamical system was presented in [4].

An ES controller applies an additive input sinusoidal perturbation [20] to the best guess of the optimum. This results in a function $f(\mathbf{x})$ that varies cyclically around a mean value. The measurement of the function $f(\mathbf{x})$ is passed through a high-pass filter to remove this mean, followed by multiplication with the perturbation. This delivers an estimate of the gradient of the function to the perturbed signal. This gradient is used to take a step towards the optimum. This is repeated until convergence.

C. Different Engine Faults and Disturbances

An engine is a complex electro-mechanical system with thousands of moving parts working together to generate the desired torque. A small fault in any of those subsystems can result in catastrophic failure of the complete system. The most common potential points of failure and inefficiency are due to faults in the fuel injection system, combustion cylinders, EGR and VGT subsystems, leaks in the intake manifold, exhaust manifold, disturbances in the SOI [8], and engine operation under non-calibrated setpoints. The main focus of this paper is to develop an online mitigation methodology for these different scenarios. The different types of faults we consider in the fuel injection system and their impact on the overall system are described below:

- Fuel injector nozzle erosion due to cavitation - This affects the atomization, mixing, and combustion inside the cylinders and thus the engine torque.

- Fuel injector nozzle clogging - This would elongate/delay the combustion and thus the amount of torque generation.
- Incorrect timing/movement of injector solenoid valve - Change in injection timing directly affects the amount of fuel injection in the cylinders resulting in a change in torque. This can cause vibrations also if the amount of fuel injected is different for one cylinder.
- Incorrect pressure supply from fuel pump - Increased/decreased injection pressure directly affects the amount of fuel inserted into the cylinders.

In this paper, we particularly focus on cavitation and clogging of fuel injectors, which can be simulated by increasing and decreasing the area of the injector nozzle, respectively. We also show the result of a disturbance at SOI due to the incorrect opening time of the injector solenoid valve and engine operation in a non-calibrated setpoint. The impact of these different scenarios can be minimized by optimizing the three control actions considered in the paper, namely, injection pressure (u_{Pinj}), injection duration (u_{tinj}), and the start of injection (u_{SOI}).

IV. Engine Control Calibration using Bayesian Optimization

We used BO to generate the control calibration map using the hybrid diesel engine model which was calibrated with experimental data. BO has been used previously in [21] to generate the engine calibration map. The map is generated by optimizing the fuel efficiency $\dot{m}_f$ for different engine operating points.

The speed operating points were chosen as 1000, 1100, 1200, 1300, 1400, 1500 and 1600 rpm and the torque operating points were chosen as 100, 150, 200, 250, 300, 350, 400, 450, and 500 Nm. The engine calibration is carried out at a steady-state operating condition with fixed speed (n_e) and torque (M_e). The relation between the fuel consumption rate and the engine inputs under an operating condition is defined as $\dot{m}_f(\mathbf{u}, n_e, M_e)$, where $\mathbf{u} = [u_1, u_2, u_3]$ are controllable engine parameters, denoted as:

$$u_1 = u_{Pinj}, \quad u_2 = u_{tinj}, \quad u_3 = u_{SOI}.$$

The steady-state torque is set as a constraint in addition to the constraints on the inputs $\mathbf{u}$. The optimization problem used for engine calibration is described as:

$$\begin{aligned}
&\text{Minimize } \dot{m}_f(\mathbf{u}, n_e, M_e) \\
&\text{subject to } M_e^s - \delta \leq M_e(\mathbf{u}, n_e, \dot{m}_f) \leq M_e^s + \delta, \\
&\qquad n_e = n_e^s, \\
&\qquad \mathbf{u} = [u_1, u_2, u_3], \\
&\qquad \text{Inj. pressure}_{\min} \leq u_1 \leq \text{Inj. pressure}_{\max}, \\
&\qquad \text{Inj. duration}_{\min} \leq u_2 \leq \text{Inj. duration}_{\max}, \\
&\qquad \text{SOI}_{\min} \leq u_3 \leq \text{SOI}_{\max}. \qquad (5)
\end{aligned}$$

The variables n_e^s, and M_e^s are the setpoint speed and torque. In the problem formulation, eq. (5), the torque constraint is relaxed to inequality constraints with a small number δ.

TABLE II: Simulation Setup for Engine Calibration

	Parameters	Range
Calibration Variables	Inj. pressure	[4 - 25] MPa
	Inj. duration	[0.3 - 3] ms
	SOI	[345 - 380] CAD
Constraint	Torque (M_e)	$[M_e^s - \delta, M_e^s + \delta]$
Objective	$\dot{m}_f$	–

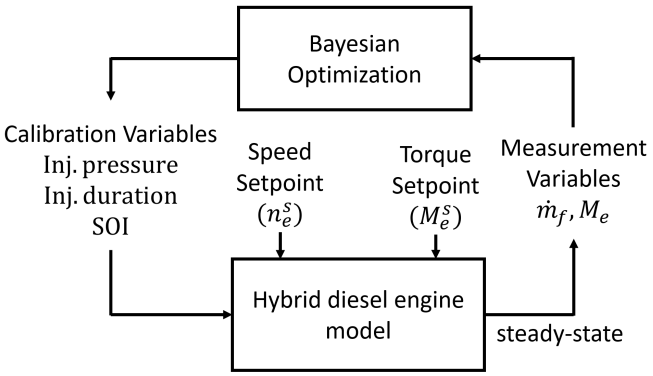

Fig. 2: Architecture for engine calibration

The value of δ chosen for this problem is 0.3 Nm. The main objective of the optimization eq. (5) is to minimize the fuel consumption rate $\dot{m}_f$ for a particular engine torque M_e^s and engine speed n_e^s. The control parameters $\mathbf{u}$ affect the combustion phase, thereby affecting the torque and fuel consumption rate. Table II shows the complete simulation setup with all engine variables and their respective constraints used for the optimization problem formulated in eq. (5).

Fig. 2 illustrates the architecture implemented to perform the engine calibration process. The BO algorithm is implemented in MATLAB script to perform the optimization. The script is used to develop a surrogate model and generate the next query points for model refining. The query points generated are the possible optimal test points, also called calibration variables. These points are then evaluated using the hybrid diesel engine model. The system is allowed to obtain a steady state, after which the desired measurement variables are fed back again to the script. This process is continued until the total evaluation budget is reached. The script then provides the optimum input $\mathbf{u}^*$ at the end. This process is repeated for all the 63 operating points obtained with the combination of speeds and torque values.

Fig. 3 illustrates the optimized fuel consumption rate for all the 63 operating points. It can be seen from the figure that as the torque is increased, the fuel consumption rate also increases to meet the increased torque demand. The figure also illustrates that for a fixed torque, as the engine speed increases, the fuel consumption rate also increases.

V. Hierarchical Control for Online Fault Mitigation

The control calibration map is generated offline with the hybrid engine model. Therefore the optimized values of the

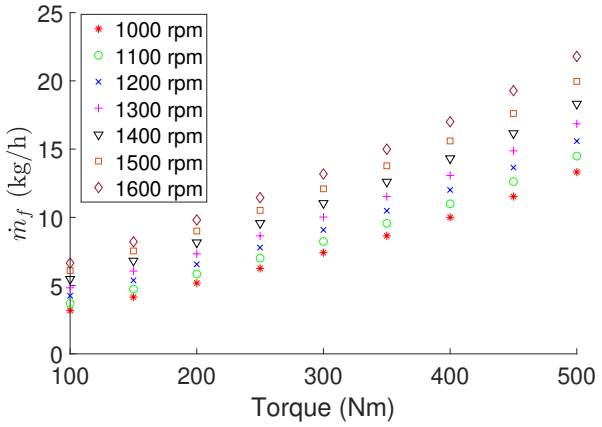

Fig. 3: Optimized fuel consumption rate

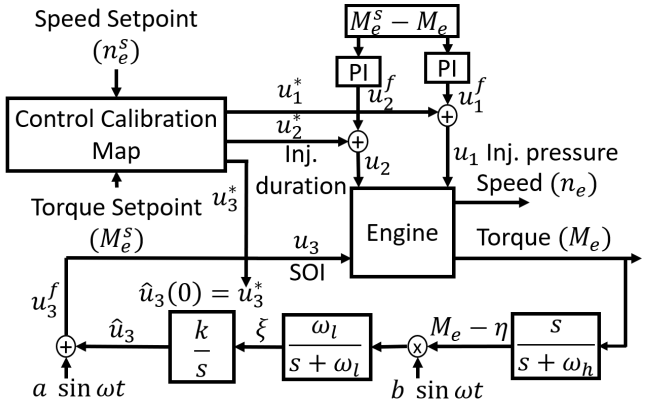

Fig. 4: Control architecture for online engine calibration

engine control parameters are prone to modeling errors and not responsive to engine faults, as discussed in the previous section. If faults occur during the engine's operation, there will be a requirement for online tuning of the engine control parameters. In this section, we propose a PI+ES controller for optimization of the engine control parameters in cases of modeling errors and engine faults.

The overall control architecture is shown in Fig. 4. For a particular speed (n_e^s) and torque (M_e^s) setpoint, the control calibration map generates the optimal engine control parameters. However, due to modeling errors and engine faults, the generated optimal engine control parameters might not achieve the desired torque setpoint M_e^s. A proportional-integral (PI) feedback controller maintains the torque at the desired setpoint. The PI controller uses the tracking error $M_e^s - M_e$ to change the injection duration and injection pressure. The PI controllers can be described as:

$$u_1^f = k_p^1(M_e^s - M_e) + k_i^1 \int (M_e^s - M_e)dt, \tag{6}$$

$$u_2^f = k_p^2(M_e^s - M_e) + k_i^2 \int (M_e^s - M_e)dt. \tag{7}$$

A PI controller can also be used to control the SOI to maintain the desired torque using the following:

$$u_3^f = k_p^3(M_e^s - M_e) + k_i^3 \int (M_e^s - M_e)dt. \tag{8}$$

However, the PI controller might not produce the optimal changes required to minimize the fuel consumption rate and maintain the desired torque. Therefore, we use an extremum seeking (ES) controller to change the SOI online to minimize the fuel consumption rate. The ES controller changes the SOI to maximize the torque M_e. As the torque is maximized by controlling the SOI, the PI controller decreases the injection pressure and duration to maintain the same desired torque, which in turn decreases the fuel consumption rate. This approach helps achieve optimal online calibration by changing the SOI using the ES controller. The ES controller can be described as:

$$\dot{\eta} = -\omega_h \eta + \omega_h M_e, \tag{9a}$$

$$\dot{\xi} = -\omega_l \xi + \omega_l (M_e - \eta) b \sin \omega t, \tag{9b}$$

$$\dot{\hat{u}}_3 = k\xi, \tag{9c}$$

$$u_3^f = \hat{u}_3 + a \sin \omega t, \tag{9d}$$

where ω_h, ω_l, and ω are the frequencies of the high-pass filter, low-pass filter, and the perturbation signal. The modulation amplitude is given by a, and the demodulation amplitude is given by b. The adaptation gain is given by k. ξ and η are the low-pass and high-pass filter states. Finally, $\hat{u}_3$ represents the mean perturbation. The initial condition of the integrator is chosen as $\hat{u}_3(0) = u_3^*$.

From Fig. 4, it can be seen that a sinusoidal perturbation $a \sin \omega t$ is added to the estimate of the optimum $\hat{u}_3$ resulting in the modulated signal u_3^f, which is applied to the engine model. This results in a sinusoidal perturbation in the torque output M_e, which varies about some mean value. The torque M_e is high-pass filtered to remove the mean (DC component) resulting in the oscillatory signal $M_e - \eta$. The high-pass filter frequency ω_h is chosen to pass the perturbation frequency ω. The high-pass filtered signal is then multiplied by the signal $b \sin \omega t$, resulting in the demodulated signal ξ. The signal ξ measures gradients in the objective function. The demodulated signal is then integrated into $\hat{u}_3$ with the integration gain k.

The engine control parameters then fed to the engine are given as:

$$u_1 = u_1^f + u_1^*,\ u_2 = u_2^f + u_2^*,\ u_3 = u_3^f,$$

where u_1^*, u_2^*, and u_3^* represents the engine control parameters generated from the engine control map.

VI. Results

In this section, we compare the performance of the PI+ES controller with the PI controller for online calibration when there are engine faults.

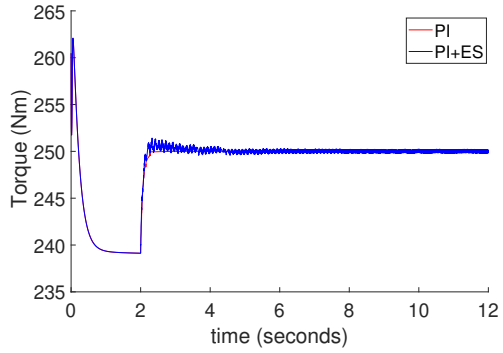

(a) Engine torque with step disturbance in SOI

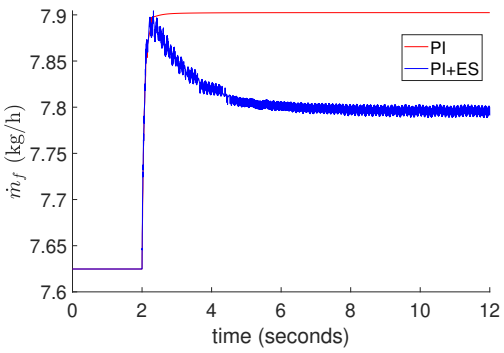

(b) Fuel consumption rate with step disturbance in SOI

Fig. 5: Comparison of engine torque and fuel consumption rate with PI and PI+ES controller under SOI step disturbance

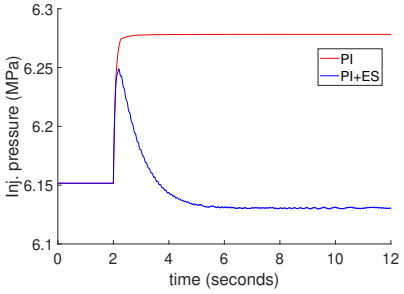

(a) Inj. pressure with step disturbance in SOI

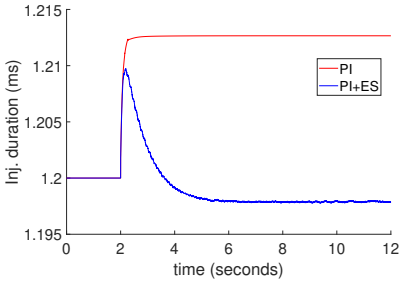

(b) Inj. duration with step disturbance in SOI

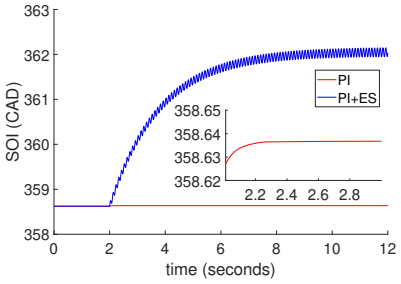

(c) SOI under step disturbance

Fig. 6: Comparison of engine injection parameters with PI and PI+ES controller under SOI step disturbance

A. *Step disturbance in SOI*

We tested the PI and PI+ES controller for the case when there is a step disturbance in the SOI value. The speed and torque setpoints were 1200 rpm and 250 Nm, respectively. The size of the step disturbance is $\Delta = 5$ CAD. The engine is initialized with $u_1^* = 6.15$ MPa, $u_2^* = 1.2$ ms, and $u_3^* = 363.62 - \Delta = 358.62$ CAD obtained from the control calibration map for the chosen setpoints. The PI and ES controller parameters are given by $k_p^1 = 10^3$, $k_i^1 = 10^6$, $k_p^2 = 10^{-3}$, $k_i^2 = 0.1$. $k_p^3 = 10^{-3}$, $k_i^3 = 0.1$, $k = 15$, $\omega_l = 0.2\pi$, $\omega_h = 0.1\pi$, $\omega = 20\pi$, $a = 0.1$, $b = 0.2$. The controller parameters were chosen from simulation such that the convergence of the ES controller to the optimum is fast.

The system is allowed to reach a steady state (first two seconds), after which the feedback controllers are turned on. Due to the step disturbance in the SOI value, the torque generated by the engine does not reach the desired setpoint as seen in Fig. 5a during the first two seconds. Both the PI and PI+ES controllers were able to achieve the desired torque. The fuel consumption rate achieved by the PI+ES controller is lower than the PI controller to achieve the same desired torque as illustrated in Fig. 5b. The lower fuel consumption rate is because the injection pressure and injection duration using the PI+ES controller are lower than with the PI controller, as seen in Fig. 6a and Fig. 6b. Finally, the lower values of injection pressure and duration are a result of the fact that the SOI using the PI+ES controller converges to a value that is much closer to the original optimal value $u_3^* = 363.62$ CAD compared to the PI controller, which converged to a value of 358.63 CAD which is far away from optimum as seen in Fig. 6c. This illustrates that the PI+ES controller can achieve optimal online calibration. Table III illustrates the steady state values of the engine control parameters.

TABLE III: Steady-state values obtained from online calibration with step disturbance in SOI

Controller	Inj. Pressure (MPa)	Inj. Duration (ms)	SOI (CAD)	$\dot{m}_f$ (kg/h)	Torque (Nm)
PI	6.27	1.21	358.63	7.90	250.01
PI+ES	6.13	1.19	362.04	7.78	249.98

B. *Non-calibrated Setpoint*

To test the controller's performance for non-calibrated setpoints, we chose the operating speed and torque as 1200 rpm and 600 Nm, respectively. This setpoint is not covered in the calibration map. We use the engine control parameters for the speed and torque operating point of 1200 rpm and 500 Nm, which is in the calibration map. The optimal engine control parameters are given by $u_1^* = 13.91$ MPa, $u_2^* = 1.2$ ms, and $u_3^* = 363.22$ CAD. The PI and ES controller parameters are given by $k_p^1 = 10^2$, $k_i^1 = 10^5$, $k_p^2 = 10^{-4}$, $k_i^2 = 0.01$. $k_p^3 = 10^{-4}$, $k_i^3 = 0.01$, $k = 2$, $\omega_l = 0.2\pi$, $\omega_h = 0.1\pi$, $\omega = 10\pi$, $a = 0.4$, $b = 0.9$. Similar

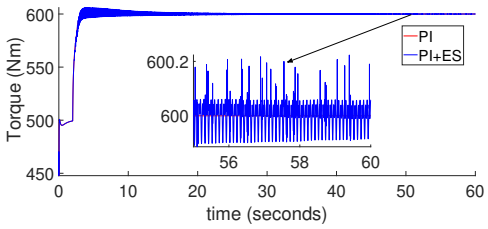

(a) Engine torque for non-calibrated setpoint

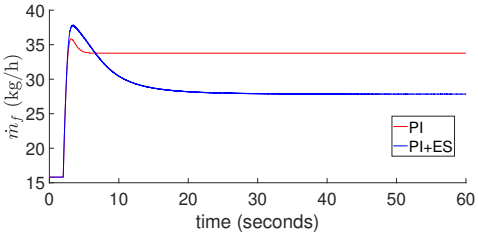

(b) Fuel consumption rate for non-calibrated setpoint

Fig. 7: Comparison of engine torque and fuel consumption rate with PI and PI+ES controller under non-calibrated setpoint

TABLE IV: Steady-state values obtained from online calibration with non-calibrated setpoint

Controller	Inj. Pressure (MPa)	Inj. Duration (ms)	SOI (CAD)	$\dot{m}_f$ (kg/h)	Torque (Nm)
PI	18.06	1.61	363.64	33.76	600.01
PI+ES	16.97	1.50	357.50	27.84	599.98

to the case, the controller parameters were chosen from simulation such that the convergence of the ES controller to the optimum is fast. Both controllers achieved the desired torque as seen in Fig. 7a. The fuel consumption rate for the PI+ES controller is less than the PI controller as seen in Fig. 7b. Table IV illustrates the steady state values of the engine control parameters achieved when using the controllers. The injection pressure is higher for the PI controller, while the SOI is lower for the PI+ES controller.

C. Area Fault

In this section, we first test the performance of the controllers for the case when the fuel injector nozzle has clogged by 20%. We chose the operating speed and torque as 1600 rpm and 500 Nm, respectively. The engine control parameters from the calibration map are given by $u_1^* = 14.42$ MPa, $u_2^* = 1.2$ ms, and $u_3^* = 361.2461$ CAD. The PI and ES controller parameters are given by $k_p^1 = 10^3$, $k_i^1 = 10^6$, $k_p^2 = 10^{-3}$, $k_i^2 = 0.1$. $k_p^3 = 10^{-3}$, $k_i^3 = 0.1$, $k = 6$, $\omega_l = 0.2\pi$, $\omega_h = 0.1\pi$, $\omega = 2\pi$, $a = 0.01$, $b = 0.05$. The controller parameters were chosen from simulation such that the convergence of the ES controller to the optimum is fast. Due to the clogging of the fuel injector, the amount of fuel injected into the cylinder is reduced which results in a lower torque output. This is illustrated in Fig. 8 where the engine torque is not able to attain the desired torque setpoint during the first two seconds before feedback control is engaged. AS seen from Fig. 8 both the PI and PI+ES controllers achieved the desired setpoint torque. The fuel consumption rate is slightly lower for the PI+ES controller (22.17 kg/h) than for the PI controller (22.39 kg/h). Similar to the previous case, the injection pressure is higher for the PI controller (15.41 MPa) than the PI+ES controller (15.34 MPa). At the same time, the SOI is higher for the PI+ES controller (365.22 CAD) than the PI controller (361.34 CAD).

Table V illustrates the performance of the PI+ES controller and provides the obtained steady state values of the engine

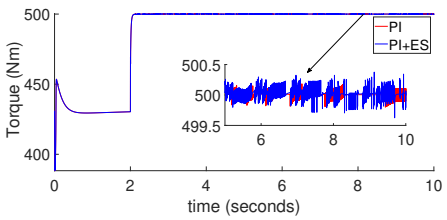

Fig. 8: Engine torque for area fault

TABLE V: Steady-state values obtained from online calibration with area clogging and erosion fault with engine setpoints of 1600 rpm and 500 Nm

Fault % (Area) (PI+ES)	Inj. Pressure (MPa) (PI+ES)	Inj. Duration (ms) (PI+ES)	SOI (CAD) (PI+ES)	$\dot{m}_f$ (kg/h) (PI+ES)	$\dot{m}_f$ (kg/h) (PI)
30 (clogging)	16.02	1.35	365.21	22.08	22.30
40 (clogging)	16.83	1.44	365.21	21.99	22.19
50 (clogging)	17.82	1.54	365.21	21.90	22.08
30 (erosion)	12.95	1.05	365.21	22.51	22.77
40 (erosion)	12.59	1.01	365.22	22.58	22.83
50 (erosion)	12.25	0.98	365.22	22.65	22.88

control parameters for a wide range of clogging/erosion in the fuel injector nozzle. For all the cases, the SOI converges to the same value. The injection pressure and duration are higher for area clogging fault as less fuel comes out of the fuel injector. On the other hand, the injection pressure and duration are lower for area erosion faults as more fuel comes out of the fuel injector. Compared to the PI controller, the PI+ES controller has lower fuel consumption rate. Although using the PI+ES controller results in a slightly lower fuel consumption rate than the PI controller, but the effect on total fuel consumption would be significantly accentuated for long operation times. The slight increase in fuel efficiency would have even more significant impact when the diesel engine is being used for longer duration ship missions with limited fuel and hard time constraints, as just a slight reduction in fuel availability can force the ship to miss important visiting points on the mission plan.

VII. Conclusion

We proposed a hierarchical control structure where a control calibration map is generated to find the optimal engine control parameters to minimize the fuel consumption

rate for different operating conditions of speed and torque. This map is generated offline using Bayesian optimization with a high fidelity hybrid engine model. We then use a proportional-integral (PI) and extremum seeking (ES) controller to compensate for modeling errors and engine faults. The PI controller controls the injection pressure and duration and maintains the torque at the desired setpoint. In contrast, the ES controller is used for optimal online calibration of the SOI to maximize the torque when the PI controller outputs reach a steady state. As the torque increases, the PI controllers lower the injection pressure and duration to maintain the torque at the desired setpoint, which minimizes the fuel consumption rate. We considered three scenarios for testing the efficiency of the PI+ES controller. The PI+ES controller lowered the fuel consumption rate for all three scenarios compared to the PI controller by optimally changing the engine control parameters online.

ACKNOWLEDGEMENT

This work was supported by the Office of Naval Research Science of Artificial Intelligence program under contract N00014-20-C-1065. The authors would like to thank Professor Benjamin Lawler from Clemson University for the insightful discussions.

REFERENCES

[1] G. Vachtsevanos, B. Lee, S. Oh, and M. Balchanos, "Resilient design and operation of cyber physical systems with emphasis on unmanned autonomous systems," *Journal of Intelligent & Robotic Systems*, vol. 91, no. 1, pp. 59–83, 2018.

[2] J. Banks, J. Hines, M. Lebold, R. Campbell, and C. Begg, "Failure modes and predictive diagnostics considerations for diesel engines," PENNSYLVANIA STATE UNIV UNIVERSITY PARK APPLIED RESEARCH LAB, Tech. Rep., 2001.

[3] Q. Tan, P. S. Divekar, Y. Tan, X. Chen, and M. Zheng, "Pressure sensor data-driven optimization of combustion phase in a diesel engine," *IEEE/ASME Transactions on Mechatronics*, vol. 25, no. 2, pp. 694–704, 2020.

[4] M. Krstić and H.-H. Wang, "Stability of extremum seeking feedback for general nonlinear dynamic systems," *Automatica*, vol. 36, no. 4, pp. 595–601, 2000.

[5] S. Kitazono, S. Sugihira, and H. Ohmori, "Starting speed control of si engine based on extremum seeking control," *IFAC Proceedings Volumes*, vol. 41, no. 2, pp. 1036–1041, 2008.

[6] N. J. Killingsworth, S. M. Aceves, D. L. Flowers, F. Espinosa-Loza, and M. Krstic, "Hcci engine combustion-timing control: Optimizing gains and fuel consumption via extremum seeking," *IEEE Transactions on Control Systems Technology*, vol. 17, no. 6, pp. 1350–1361, 2009.

[7] E. Corti, C. Forte, G. Mancini, and D. Moro, "Automatic combustion phase calibration with extremum seeking approach," *Journal of Engineering for Gas Turbines and Power*, vol. 136, no. 9, 2014.

[8] E. Hellstrom, D. Lee, L. Jiang, A. G. Stefanopoulou, and H. Yilmaz, "On-board calibration of spark timing by extremum seeking for flex-fuel engines," *IEEE Transactions on control systems technology*, vol. 6, no. 21, pp. 2273–2279, 2013.

[9] D. Popovic, M. Jankovic, S. Magner, and A. R. Teel, "Extremum seeking methods for optimization of variable cam timing engine operation," *IEEE Transactions on Control Systems Technology*, vol. 14, no. 3, pp. 398–407, 2006.

[10] X. Shen, Y. Zhang, T. Shen, and C. Khajorntraidet, "Spark advance self-optimization with knock probability threshold for lean-burn operation mode of si engine," *Energy*, vol. 122, pp. 1–10, 2017.

[11] Q. Tan, P. Divekar, Y. Tan, X. Chen, and M. Zheng, "Model-guided extremum seeking for diesel engine fuel injection optimization," *IEEE/ASME Transactions on Mechatronics*, vol. 23, no. 2, pp. 936–946, 2018.

[12] X. Yu, L. Zhu, Y. Wang, D. Filev, and X. Yao, "Internal combustion engine calibration using optimization algorithms," *Applied Energy*, vol. 305, p. 117894, 2022.

[13] F. Kupper, A. Forrai, A. Indrajuana, R. van der Weijst, T. van Keulen, and F. Willems, "Robust fuel consumption estimation for on-line optimization of diesel engines," *IFAC-PapersOnLine*, vol. 51, no. 31, pp. 233–239, 2018.

[14] J. B. Heywood, *Internal combustion engine fundamentals*. McGraw-Hill Education, 2018.

[15] N. Watson, "Dynamic turbocharged diesel engine simulator for electronic control system development," 1984.

[16] A. G. Stefanopoulou, I. Kolmanovsky, and J. S. Freudenberg, "Control of variable geometry turbocharged diesel engines for reduced emissions," *IEEE transactions on control systems technology*, vol. 8, no. 4, pp. 733–745, 2000.

[17] F. Maroteaux and C. Saad, "Combined mean value engine model and crank angle resolved in-cylinder modeling with nox emissions model for real-time diesel engine simulations at high engine speed," *Energy*, vol. 88, pp. 515–527, 2015.

[18] J. Wahlström and L. Eriksson, "Modelling diesel engines with a variable-geometry turbocharger and exhaust gas recirculation by optimization of model parameters for capturing non-linear system dynamics," *Proceedings of the Institution of Mechanical Engineers, Part D: Journal of Automobile Engineering*, vol. 225, no. 7, pp. 960–986, 2011.

[19] B. Shahriari, K. Swersky, Z. Wang, R. P. Adams, and N. De Freitas, "Taking the human out of the loop: A review of bayesian optimization," *Proceedings of the IEEE*, vol. 104, no. 1, pp. 148–175, 2015.

[20] K. B. Ariyur and M. Krstic, *Real-time optimization by extremum-seeking control*. John Wiley & Sons, 2003.

[21] A. Pal, L. Zhu, Y. Wang, and G. G. Zhu, "Constrained surrogate-based engine calibration using lower confidence bound," *IEEE/ASME Transactions on Mechatronics*, vol. 26, no. 6, pp. 3116–3127, 2021.

APPENDIX

u_{Pinj}	Common rail injection pressure (MPa)
$\dot{m}_c$	Compressor mass flow (Kg/sec)
T_{em}	Cylinder exhaust temperature (K)
T_{im}	Cylinder intake temperature (K)
$\dot{m}_{ci}$	Cylinder in mass flow (Kg/sec)
$\dot{m}_{co}$	Cylinder out mass flow (Kg/sec)
P_{cyl}	Cylinder pressure (Pa)
C_d	Discharge coefficient for injector (mm)
n_e	Engine speed (RPM)
R_e	Exhaust ideal-gas constant (J/KgK)
P_{em}	Exhaust manifold pressure (Pa)
V_{em}	Exhaust manifold volume (m^3)
ρ	Fuel density (Kg/m^3)
A_{flow}	Injector nozzle area (m^2)
u_{tinj}	Injection duration (ms)
R_a	Intake ideal-gas constant (J/KgK)
P_{im}	Intake manifold pressure (Pa)
V_{im}	Intake manifold volume (m^3)
u_{SOI}	Start of injection $(crank\ angle\ degree)$
M_e	Torque (Nm)
$\dot{m}_t$	Turbine mass flow (Kg/sec)